

Modeling and Control of a New Actuation Mechanism for Interfacial Force Microscopy*

A. Mesbah-Nejad, M. Moallem and R.V. Patel**

Abstract—In this paper, a new model for a capacitance-based force sensor used in Interfacial Force Microscopy (IFM) is proposed. This model considers both rotation and bending of the torsion bars of a teeter-totter mechanism. A new actuation method is introduced which greatly reduces the stress and strain of the torsion bars. This results in increased sensitivity of the sensor. A dynamic output feedback controller for this actuation scheme is utilized in which the only measurement required is the position of the sensor. Simulation results are presented that confirm the analytical results.

I. INTRODUCTION

Atomic force microscope (AFM) is an instrument invented in 1986 [1] for studying surface properties of materials at the atomic level. AFM and its variations have been widely used to probe a large range of physical and biological processes in different research areas including mechanical properties of single molecules, electric and magnetic fields of single atoms and electrons, fabrication of microscopic devices, DNA analysis and dissection, polymers and biomaterials analysis, materials science, nano-manipulation, microelectronics, telecommunications, data storage, and many other high-tech industries. It has opened new perspectives in the investigation and manipulation of biomedical specimens by looking at, and working on, samples with “atomic” resolution images which contain details not observable using any other instrument.

In AFM, the interfacial force is measured by measuring the deflection of a cantilever beam. This method is simple and sensitive, but has some disadvantages. The force measurement changes the interfacial separation and does not give a direct measure of the force versus distance [2]. Another problem appears when the spring constant is low and the speed of approach or retraction is large. In such a case, the sensor may become unstable due to the nonlinearity of the interaction force [2]. Finally, the measurement of force involves elastic energy storage in the sensor. Thus, if the sensor moves to the thinner parts of the sample, the released energy makes it difficult to study the topography of the sample [2]. Interfacial Force Microscope (IFM) developed by Joyce *et al.* [3], [4] is a modification of AFM with superior capabilities for measuring force-displacement curves. Figure

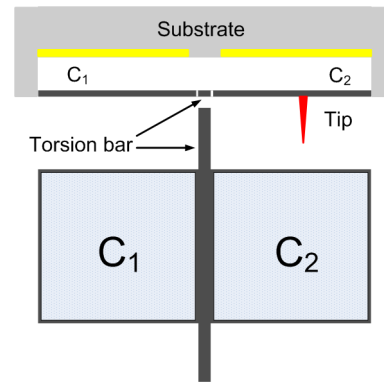


Fig. 1. Schematic diagram of IFM force sensor.

1 shows the IFM force sensor introduced by Joyce and Houston [3]. The force is detected by sensing the deflection of the tip and a force compensation system returns the sensor tip to its original position. In this method, the electrostatic forces generated by the capacitors are used to compensate for the interaction forces; hence the sensor has effectively zero-compliance. The deflection can be detected by measuring the changes in the capacitance values or with other optical methods.

IFM is a very suitable tool for biomedical applications because of its longer and more rigid tungsten tip when compared to AFM, which makes it easy to use inside watery environments without significant changes in its characteristics. IFM can be used for both indentation and imaging applications. This makes IFM a unique scientific instrument.

In the current IFM sensor the electrostatic force is always attractive. Currently in order to compensate for repulsive forces, a DC bias voltage is applied on both capacitors. The measuring range of the sensor is proportional to the magnitude of the DC bias. The problem is that applying this voltage may result in the bending, as well as downward displacement of the common plate. The sensitivity of the sensor is inversely related to this bias voltage as well. The torsion bars can be designed to have a small torsional spring constant and large bending (up or down) spring constants. However, the common plate still moves as a result of the applied forces [2].

Despite the current achievements in this area, IFM needs to be improved in terms of speed, sensitivity, and sensor design to be competitive with the available commercial instruments. In this work, our focus is to develop a new actuation and control scheme in order to achieve a higher sensitivity of the microscope without reducing its measuring range.

*This research was supported by the Natural Sciences and Engineering Research Council (NSERC) of Canada under grants RGPIN-1345 and RGPIN-227612.

**A. Mesbah-Nejad and R.V. Patel are with the Department of Electrical and Computer Engineering, The University of Western Ontario, London, Ontario, N6A 5B9, Canada amesbahn@uwo.ca, rajni@eng.uwo.ca

M. Moallem is with the School of Engineering Science, Simon Fraser University, Surrey BC, V3T 0A3, Canada mmoallem@sfu.ca

II. IFM FORCE SENSOR MODEL

Figure 2 shows the schematic diagram of the common plate of the IFM force sensor. The torsion bars are connected to the common plate from one side and to the frame (fixed points) from the other side. Although the torsion bars are designed to have relatively high spring constants in the Z and Y directions compared to their torsional spring constant, they still may bend when electrostatic and interfacial forces are applied to the sensor. Considering the direction of the applied forces, the bending in the Y direction can be neglected while the movement of the plate in the Z direction should be considered. The common plate and torsion bars can be

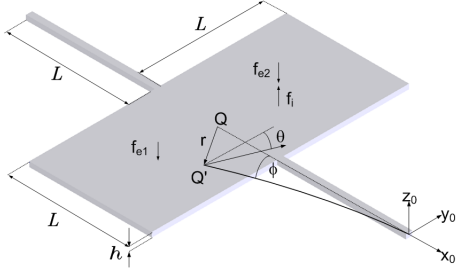


Fig. 2. Schematic diagram of the common plate of the IFM force sensor.

modelled by a mass located at the center and four springs (two torsional and two linear springs). The parameters and coordinates chosen for this case are shown in Figure 2. The equations of the motion of the tip of the sensor can be derived from the Lagrangian formulation [5]

$$\frac{d}{dt} \frac{\partial L}{\partial \dot{q}} - \frac{\partial L}{\partial q} = \tau \quad (1)$$

with the Lagrangian L defined in terms of the kinetic energy K and the potential energy P as $L = K - P$, q is the generalized coordinate vector and τ is the applied torque vector. Assuming that the plate is rigid, the kinetic energy of the system can be expressed as

$$\begin{aligned} K &= \frac{1}{2} m V_c^T V_c + \frac{1}{2} \omega^T I \omega \\ &= \frac{1}{2} m \left(\frac{dr^T}{dt} \right) \left(\frac{dr}{dt} \right) + \frac{1}{2} \omega^T I \omega \end{aligned} \quad (2)$$

where m is mass of the moving part (plate and tip and torsion bars), V_c is the velocity vector of the center of mass of the plate, r is the position vector of the center of mass of the common plate (\dot{Q}) with reference to its original position (Q), ω is the angular velocity of the common plate, and I is the inertia tensor of the common plate with reference to its center of mass (\dot{Q}). To simplify the dynamic equations of motion, from now on we assume that $L_t = 2L_a = L$ where L_t is the length of the torsion bars, L_a is the distance from the tip to the axis of torsion bars, and L is the side length of each capacitor plate. The movement of the tip in the z direction is a consequence of the bending of the torsion bars and the rotation of the common plate. The bending and twist angles are shown in Figure 2 by ϕ and θ , respectively. Assuming that ϕ and θ are very small, these movements can

be approximated by $\frac{3L}{2}\phi$ and $\frac{L}{2}\theta$ and the total displacement of the tip is

$$z = \frac{3L}{2}\phi + \frac{L}{2}\theta. \quad (3)$$

The inertia tensor is then calculated, as

$$I = \begin{pmatrix} I_{xx} & 0 & 0 \\ 0 & I_{yy} & 0 \\ 0 & 0 & I_{zz} \end{pmatrix}$$

and consequently the kinetic energy of the tip body is given by

$$K = \frac{1}{2} m \dot{r}^2 + \frac{1}{2} I_{xx} \dot{\theta}^2 = \frac{9}{8} m L^2 \dot{\phi}^2 + \frac{1}{2} I_{xx} \dot{\theta}^2 \quad (4)$$

where I_{xx} is the axial mass moment of inertia about the x axis. The potential energy is given by

$$\begin{aligned} P &= 2 \left(\frac{1}{2} k_b r^2 + \frac{1}{2} k_t \theta^2 \right) + mgr \\ &= \frac{9}{4} k_b L^2 \phi^2 + k_t \theta^2 + \frac{3}{2} mgL\phi \end{aligned} \quad (5)$$

where k_b and k_t are the bending and torsional spring constants of the torsion bars. The first term is the potential energy of the bending, the second term is the potential energy of the rotation, and the last term is the gravitational potential energy. The first two terms are multiplied by two as there are two torsion bars in the system.

Substituting K and P from (4) and (5) in (1), the equations of motion can be written as

$$\begin{aligned} \frac{9}{4} m L^2 \ddot{\phi} + \frac{9}{2} L^2 k_b \phi + \frac{3}{2} m L g = \\ \frac{3L}{2} [f_{e1}(z) + f_{e2}(z) - f_i(z_s - z)] \end{aligned} \quad (6)$$

$$I_{xx} \ddot{\theta} + 2k_t \theta = \frac{L}{2} [f_{e1}(z) - f_{e2}(z) - f_i(z_s - z)] \quad (7)$$

where $f_{e1}(z)$ and $f_{e2}(z)$ are the electrostatic forces exerted on the capacitors and $f_i(z_s - z)$ is the interfacial force exerted by the sample. To simplify the analysis in deriving the above equations, the widths of the torsion bars are neglected compared to the width of capacitor plates (the widths of torsion bars are around one percent of the width of capacitor plates).

The gravitational force $\frac{3}{2} m L g$ in (6) is constant and can be compensated for by a constant voltage. Therefore, it can be removed from the dynamics. Assuming an air damping force with a damping coefficient β_b for the normal movement and β_t for the rotational movement, (6) and (7) can be written as

$$\begin{aligned} \frac{9}{4} m L^2 \ddot{\phi} + \beta_b \dot{\phi} + \frac{9}{2} L^2 k_b \phi \\ = \frac{3L}{2} [f_{e1}(z) + f_{e2}(z) - f_i(z_s - z)] \end{aligned} \quad (8)$$

$$I_{xx} \ddot{\theta} + \beta_t \dot{\theta} + 2k_t \theta = \frac{L}{2} [f_{e1}(z) - f_{e2}(z) - f_i(z_s - z)]. \quad (9)$$

It can be observed from (8) and (9) that the dynamics of the system depend on the interfacial and electrostatic forces. These forces are modeled in the following subsections.

A. Modeling Interfacial Forces

The intermolecular and surface forces of elastic solids forced into contact with each other have been studied for many years [6]. Among the available models, the Hertz model, the Derjaguin-Muller-Tupporov (DMT) model, and the Johnson-Kendall-Roberts (JKR) model are more popular. For the propose of this study, the JKR model can be used. This model considers only interactions in the contact area between the tip and the sample [7]. This model consists of the Lennard-Jones potential and a modified Hertz model. The interaction force of the Lennard-Jones model is given by

$$f_{lj}(z) = f_0 R \left(-\left(\frac{\sigma}{z}\right)^2 + \frac{1}{30} \left(\frac{\sigma}{z}\right)^8 \right) \quad (10)$$

where the tip is approximated with a ball of radius R , and spherical approximation of the molecule diameter of σ . The parameter f_0 is given by

$$f_0 = \frac{2}{3} \pi^2 \epsilon \rho_1 \rho_2 \sigma^4$$

in which ρ_1 is the density of the tip, ρ_2 is the density of the sample, and ϵ is the minimum energy of the Lennard-Jones potential. The first term in the Lennard-Jones force is the attractive Van der Waals interaction force and the second term is the repulsive Pauli force. The attractive forces are shown with negative signs while the repulsive forces are shown with positive signs. The Hertz model describes the interaction between two spheres and considers the deformation of the spheres if they are in contact. By setting the radius of the sample to infinity we get the interaction between a plane surface and a spherical tip. This model has to be modified because the resulting force has to be identical with the zero point of the Lennard-Jones potential z_0 [8]. The term z_0 can be found by setting $f_{lj} = 0$ in equation (10) which yields $z_0 = 30^{-\frac{1}{6}} \sigma$. Assuming a small indentation of the plane denoted by $|z_0 - z| \ll R$ we get

$$f_h(z) = g_0 (z_0 - z)^{3/2} \quad (11)$$

where

$$g_0 = \frac{8\sqrt{2}R}{3\pi \left(\frac{1-\nu_1^2}{\pi E_1} + \frac{1-\nu_2^2}{\pi E_2} \right)} \quad (12)$$

in which ν_1, ν_2 are the Poisson ratios of the tip and the sample, and E_1, E_2 are the Young's moduli of the tip and the sample, respectively. Combining (10) and (11) results in the interaction force for the whole range given by

$$f_i(z) = \begin{cases} f_{lj}(z) & \text{if } z > z_0 \\ f_h(z) & \text{if } z \leq z_0 \end{cases} \quad (13)$$

B. Modeling Electrostatic Forces

When the tip approaches the sample, the interaction forces pull the common plate toward the sample. In order to find electrostatic forces the value of the capacitors should be calculated first. The parallel plate capacitance is calculated by

$$C_0 = \epsilon \epsilon_0 \frac{L^2}{D} \quad (14)$$

where ϵ is the relative permittivity of the medium between two electrodes ($\simeq 1$ for air), $\epsilon_0 = 8.854 \times 10^{-12} \frac{C^2}{N.m^2}$ is the permittivity of vacuum, L^2 is the area of each electrode, and D is the gap between the plates.

Rotation of the common plate changes the air gap between the plates. Assuming that the angle of rotation is small enough, the change in the air gap can be approximated by the movement of the tip. With this assumption, the capacitance formula changes to

$$C(z) = \epsilon_0 \frac{L^2}{D - z} \quad (15)$$

where z is the movement of the tip. When a voltage is applied to a capacitor, it will be charged by $Q = C(z)V$ and the electric energy stored in the capacitor is $E = \frac{1}{2}C(z)V^2$. The electrostatic force acting on the capacitors is given by

$$f_e(z) = -\frac{dE}{dz} = -\frac{1}{2}V^2 \frac{dC}{dz} = \frac{1}{2} \frac{\epsilon_0 L^2}{(D - z)^2} V^2 \quad (16)$$

III. ACTUATION SCHEME

One common approach is to bias both capacitors with a constant DC voltage (V_{dc}) and apply a control voltage u on the one of the two capacitors and $-u$ on the other one ($u < V_{dc}$) [9], [4]. This approach is referred to as double-sided actuation. In this method, there is always a vertical displacement of the common plate which is the consequence of the DC bias voltage of the capacitors. This voltage exerts electrostatic forces on both sides of the teeter-totter mechanism. The problems of common plate displacement will be alleviated if one uses compensation only on the tip-bearing capacitor (C_2 in Figure 1). This method is referred to as single-sided actuation. In this case, both the total torque and the net vertical force are balanced. In both cases, the electrostatic forces have nonlinear relationships with the control voltage. This is not too bad for rotation control as it is possible to find a control input which can regulate the rotation but these methods cause considerable deflection of the torsion bars. For the sensor used in this study (refer to Table I), and for $f_i = 0, V_{dc} = 10$ V, with no control voltage, the constant force exerted on the sensor ($f_{e1}(z) + f_{e2}(z)$) is around $32.6 \mu N$ which generates considerable amount of stress and strain on the sensor and reduces its sensitivity.

The approach proposed in this work to resolve this problem is to use an antagonistic actuation scheme. Figure 3 shows the schematic diagram of the proposed method. In this mechanism, the controller has two outputs u_1 and u_2 . The u_2 output will be active when $z \leq 0$, while the u_1 output will be active when $z > 0$. The electrostatic force exerted on the sensor can then be calculated as

$$f_e(z) = \begin{cases} f_{e2}(z) = \frac{1}{2} \frac{\epsilon_0 L^2}{(D-z)^2} u_2^2, & z \leq 0 \\ f_{e1}(z) = \frac{1}{2} \frac{\epsilon_0 L^2}{(D+z)^2} u_1^2, & z > 0 \end{cases} \quad (17)$$

IV. CONTROLLER DESIGN

Inspecting Table (I) reveals that k_b is bigger than k_t in the order 10^5 , so ϕ can be safely ignored in (3) and consequently $|z| \approx \frac{L}{2}\theta$. Therefore, in the following analysis the bending

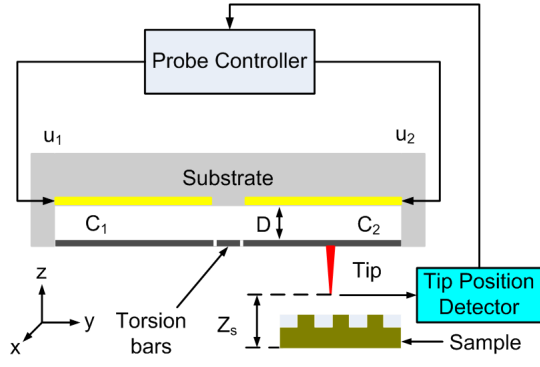


Fig. 3. Antagonistic Actuation Scheme.

dynamics are ignored. For non-contact imaging, $z \leq 0$, $f_{e1}(z) = 0$, and $f_i(z_s - z) = f_{lj}(z_s - z)$. Now let us define

$$\gamma_2(\theta) = \frac{1}{2} \frac{\varepsilon_0 L^2}{(D + \frac{L}{2}\theta)^2} \quad \text{and} \quad u_2^2 = u \quad (18)$$

so f_{e2} can be found as $f_{e2}(z) = \gamma_2(\theta)u$. Also let us define

$$f_{lj}(z_s - z) = f_2(\theta) = f_0 R \left(-\left(\frac{\sigma}{z_s - \frac{L}{2}\theta}\right)^2 + \frac{1}{30} \left(\frac{\sigma}{z_s - \frac{L}{2}\theta}\right)^8 \right). \quad (19)$$

Now the dynamic equations of motion (9) for $z \leq 0$ can be written in the form

$$\ddot{\theta} = \frac{-2k_t}{I_{xx}} \theta - \frac{\beta_t}{I_{xx}} \dot{\theta} + \frac{L}{2I_{xx}} \gamma_2(\theta)u - \frac{L}{2I_{xx}} f_2(\theta). \quad (20)$$

Choosing $x_1 = \theta(t)$, this equation can be transformed into the state space form

$$\dot{x}_1 = x_2 \quad (21)$$

$$\dot{x}_2 = \frac{-2k_t}{I_{xx}} x_1 - \frac{\beta_t}{I_{xx}} x_2 + \frac{L}{2I_{xx}} \gamma_2(x_1) \left[u - \frac{f_2(x_1)}{\gamma_2(x_1)} \right] \quad (22)$$

$$z = \frac{L}{2} x_1 \quad (23)$$

where z is the output of the system. The control problem is to regulate the output at a constant height in the presence of varying interfacial forces.

To get some insight, let us analyze the equilibrium state of the unforced system. The equilibrium points of the unforced system can be obtained from (21) to (22), by substituting $\dot{x}_1 = \dot{x}_2 = 0$ and $u = 0$, which results

$$x_1 = -\frac{L}{4k_t} f_2(x_1), \quad x_2 = 0.$$

The equilibrium points depend on spring constant of the sensor k_t and the interfacial force $f_2(x_1)$. These points can be found graphically by finding the intersections of $f_2(x_1)$ and the linear torsional force line of the sensor. Figure 4 shows the equilibrium points of x_1 for $z_s = 0.8 \text{ nm}$ and three different values of k_t . In the equilibrium position, the interfacial forces are balanced by the restoring mechanical force. The number and the position of the equilibrium points are dependent on the spring constant. For the simulated

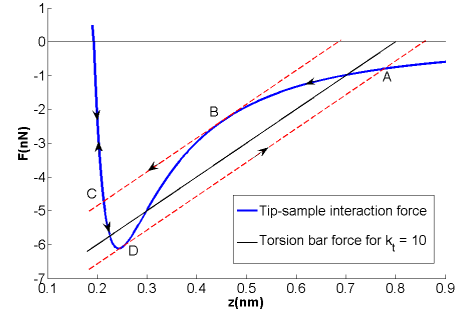


Fig. 4. force-distance curve and instability points

system with $z_s = 0.8 \text{ nm}$ and for $6 < k_t < 11 \frac{N.m}{rad}$ the number of equilibrium points varies between one to three. The typical values of the sensor parameters which have been used for simulation are listed in Table I. For the sensor to be stable, the gradient of the restoring force should be higher than that of the interfacial force. As shown in Figure 4 the gradient of the interfacial force is lower than that of the restoring force until point B is reached. At this point they are equal and after that the gradient of the interfacial force is higher, so the tip jumps to point C. In the return path, the situation is vice versa. At point D, the gradient of the restoring force is higher, hence the tip jumps off from the surface to point A. Therefore to stabilize this system, one may add the torsional stiffness of the sensor by feedback control. It can be seen from equations (21) and (22) and also from Figure 4 that the system is nonlinear. A feedback linearization approach has been used to address the nonlinearity of the system.

Let us take another pseudo control input v as

$$v = \gamma_2(x_1)u - f_2(x_1). \quad (24)$$

Substituting u from (24) in (22) converts the system to the following linear system

$$\dot{x} = Ax + Bv \quad (25)$$

$$z = Cx \quad (26)$$

with

$$A = \begin{pmatrix} 0 & 1 \\ -\frac{2k_t}{I_{xx}} & -\frac{\beta_t}{I_{xx}} \end{pmatrix}, \quad B = \begin{pmatrix} 0 \\ \frac{L}{2I_{xx}} \end{pmatrix}, \quad C = \begin{pmatrix} \frac{L}{2} & 0 \end{pmatrix}, \quad (27)$$

and $x = [x_1 \ x_2]^T$. Now taking the control signal v to be

$$v = -Kx \quad \text{with} \quad K = \begin{pmatrix} k_1 & k_2 \end{pmatrix}^T \quad (28)$$

The system will be stable as long as $A - BK$ is Hurwitz. The controller (28) requires full state information which may be restrictive due to sensor requirements. The system given by (27) is observable/controllable as long as L is not zero and I_{xx} is finite (which is the case for a physical device). Hence we use a dynamic output feedback controller that uses only one measurable parameter at the output. This greatly improves the performance of the controller as it has all

benefits of the classic derivative but it is less susceptible to noise. The proposed controller is of the form

$$\dot{\eta} = h_1\eta + h_2z \quad (29)$$

$$v = h_3\eta + h_4z \quad (30)$$

where $h_1(\leq 0)$ to h_4 are the single controller design parameters. Substituting (29) and (30) in (25) results in the following augmented system

$$\dot{\tilde{x}} = \tilde{A}\tilde{x} \quad (31)$$

with

$$\tilde{x} = \begin{pmatrix} x & \eta \end{pmatrix}^T$$

and

$$\tilde{A} = \begin{pmatrix} A + Bh_4C & Bh_3 \\ h_2C & h_1 \end{pmatrix}. \quad (32)$$

Using (30), (24) and (18), the final control inputs u_2 can be calculated from

$$u_2 = \sqrt{\frac{h_3\eta + h_4z}{\gamma_2(x_1)} + \frac{f_2(x_1)}{\gamma_2(x_1)}}. \quad (33)$$

One should note that although $f_2(x_1)$ in (33) can be reconstructed using the knowledge of the interfacial force model, it can also be considered as a disturbance and ruled out from the control law. With this assumption, (24) will change to $v = \gamma_2(x_1)u$. Substituting v and z from (33) and (26) in (30), x_1 is obtained. Now substituting x_1 in (22) with x_2 and $\dot{x}_2 = 0$, the steady-state error is given by

$$x_1 = \frac{2Lh_3\eta - 2Lf_2(x_1)}{8k_t - L^2h_4} \quad (34)$$

which can be made arbitrary small with proper selection of h_3 and h_4 . One way to completely remove the output error is to add an integral term in the controller design. With this modification, the structure of the controller is given by

$$\dot{\sigma} = z \quad (35)$$

$$\dot{\eta} = g_1\eta + g_2\sigma + g_3z \quad (36)$$

$$v = g_4\eta + g_5\sigma + g_6z. \quad (37)$$

which results in the following augmented system

$$\dot{\hat{x}} = \hat{A}\hat{x} \quad (38)$$

with

$$\hat{x} = \begin{pmatrix} x & \sigma & \eta \end{pmatrix}^T$$

and

$$\hat{A} = \begin{pmatrix} A + Bg_6C & Bg_5 & Bg_4 \\ C & 0 & 0 \\ g_3C & g_2 & g_1 \end{pmatrix}. \quad (39)$$

where g_1 to g_6 are single controller gains that are designed such that \hat{A} is Hurwitz.

For $z > 0$, $f_{e2} = 0$ and again we can define $\gamma_1(x_1)$, $f_1(x_1)$, and u from (17) and (13) as

$$\gamma_1(x_1) = \frac{1}{2} \frac{\varepsilon_0 L^2}{(D - \frac{L}{2}x)^2}, \quad u_1^2 = u \quad (40)$$

$$f_1(x_1) = g_0(z_0 - x)^{3/2}. \quad (41)$$

With these definitions the state-space representation will change to

$$\dot{x}_1 = x_2 \quad (42)$$

$$\dot{x}_2 = \frac{-2k_t}{I_{xx}}x_1 - \frac{\beta_t}{I_{xx}}x_2 + \frac{L}{2I_{xx}}\gamma_1(x_1)\left[u - \frac{f_1(x_1)}{\gamma_1(x_1)}\right] \quad (43)$$

$$z = \frac{L}{2}x_1. \quad (44)$$

A similar procedure can be used when $z < 0$.

V. SIMULATION RESULTS

The system was simulated in MATLAB/Simulink. The interfacial forces were simulated by the modified JKR force model. Assuming $\beta_t = 5.36 \times 10^{-5}$ (Kg/m²)/(rad.sec), and choosing $h_1 = -50$, $h_2 = -100$, $h_3 = -3$, and $h_4 = -1$ ensures that the system is stable (\tilde{A} is full rank and the real parts of the eigenvalues are all negative). An initial tip-sample distance of 100.2 nm was set and the simulation run time was set to 2 msec. The response of the system to a step input of 100 nm applied with 1 msec delay is shown in Figure 5. The controller output is also shown in Figure 6. As the Figure 6 shows the controller is able to follow

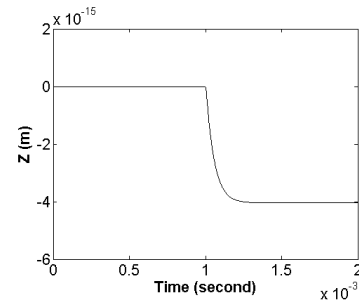


Fig. 5. Step response.

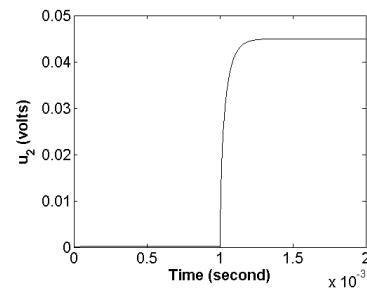


Fig. 6. Controller output to the step response.

the input very well with the transient time of less than 200 μ sec. Figure 7 shows the response of the system when a pulse disturbance with an amplitude of 0.02 volts (44% of the control signal) and pulse width of 0.5 msec is applied at 1.5 msec. The figure shows that the proposed control method is robust and can compensate for the effect of disturbances.

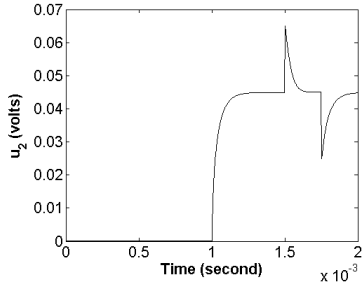


Fig. 7. Controller output with the presence of disturbance.

The step response and the output of the system after adding the integral term with $g_1 = -50$, $g_2 = -100$, $g_3 = -1$, $g_4 = -3$, $g_5 = -1 \times 10^3$, and $g_6 = -5 \times 10^3$ are shown in Figures 8 and 9. As the figures show, this

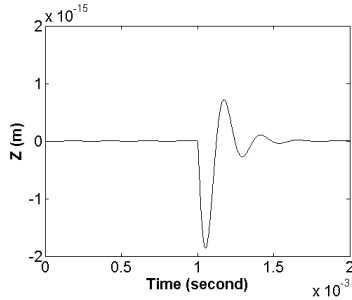


Fig. 8. Step response with integrator.

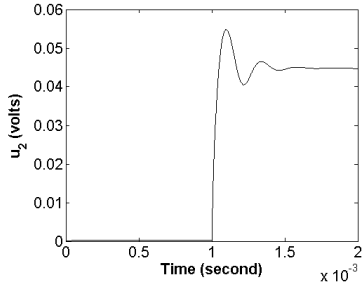


Fig. 9. Controller output with integrator.

modification completely removes the output error.

VI. CONCLUSIONS

A new model and actuation method for the IFM force sensor was introduced in this paper which considers both rotation and bending of the torsion bars of the teeter-totter mechanism. The main advantage of this method of actuation is that it completely removes the DC bias of the actuators. A dynamic feedback control scheme for this actuation scheme was designed and simulated. The results show satisfactory performance. The simulation results indicate that the proposed control scheme can greatly reduce the stress and strain of the torsion bars. However it cannot completely prevent

bending in the repulsive force regime which may reduce accuracy or cause instability in the contact mode imaging, or in the force indentation applications. This will be addressed in the future research. The experimental implementation of this control strategy is in progress.

TABLE I
TYPICAL VALUES OF THE PHYSICAL PARAMETERS OF THE FORCE
SENSOR

Parameter (Symbol)	Value for Si Sensor
ϵ_0	$8.854 \times 10^{-12} \frac{C^2}{N \cdot m^2}$
L	$2.54 \times 10^{-3} m$
ρ	$2330 \frac{Kg}{m^3}$
M	$8.2014 \times 10^{-5} Kg$
D	$5 \times 10^{-6} m$
C_0	$11.63 \times 10^{-12} F$
L_a	$1.3335 \times 10^{-3} m$
L_t	$2.667 \times 10^{-3} m$
b	$1.27 \times 10^{-4} m$
h	$1.0 \times 10^{-4} m$
E	$9.8 \times 10^{10} \frac{N}{m^2}$
ν	0.45
$G_1 = \frac{E}{2(1+\nu)}$	$3.379310 \times 10^{10} \frac{N}{m^2}$
I_{xx}	$4.415427 \times 10^{-11} Kg \cdot m^2$
I_{yy}	$6.94354 \times 10^{-10} Kg \cdot m^2$
I_{zz}	$5.510742 \times 10^{-11} Kg \cdot m^2$
dI_y	$1.734298 \times 10^{-13} m^4$
dI_z	$1.365589 \times 10^{-13} m^4$
$k_b = \frac{Eb}{4} (\frac{h}{L_t})^3$	$1.898754 \times 10^2 \frac{N}{m}$
$k_t = \frac{Ebh^3}{6L_t(1+\nu)}$	$5.632184 \times 10^{-4} \frac{N \cdot m}{rad}$

REFERENCES

- [1] G. Binning, C. F. Quate, and C. Gerber, "Atomic force microscope," *Physical Review Letters*, vol. 56, no. 9, pp. 930–933, March 1986.
- [2] J. E. Houston, *Interfacial Force Microscopy: Selected Applications*, 1st ed., ser. NanoScience and Technology. Springer, 2004, vol. Applied Scanning Probe Methodes, ch. 2, pp. 41–73.
- [3] S. Joyce, J. Houston, and B. Smith, "Interfacial force sensor with force-feedback control," *Electron Devices Meeting, Technical Digest., International*, pp. 621–624, Dec 1990.
- [4] S. A. Joyce and J. E. Houston, "A new force sensor incorporating force-feedback control for interfacial force microscopy," *Review of Scientific Instruments*, vol. 62, no. 3, pp. 710–715, March 1991.
- [5] M. W. Spong, S. Hutchinson, and M. Vidyasagar, *Robot Modelling and Control*. John Wiley & Sons, Inc., 2006.
- [6] J. Israelachvili, *Intermolecular and Surface Forces*. New York: Academic Press, 1995.
- [7] G. Schitter, P. Menold, H. F. Knapp, F. Allgöwer, and A. Stemmer, "High performance feedback for fast scanning atomic force microscopes," *Review of Scientific Instruments*, vol. 72, no. 8, pp. 3320–3326, 2001.
- [8] X. Chen and A. Lal, "Integrated pressure and flow sensor in silicon-based ultrasonic surgical actuator," in *IEEE Ultrasonics Symposium*, vol. 2, Oct 2001, pp. 1373–1376.
- [9] O. Warren, J. Graham, and P. Norton, "Tapping mode imaging with an interfacial force microscope," *Review of Scientific Instruments*, vol. 68, no. 11, pp. 4124–4130, 1997.